A 1D code for studies of divertor detachment dynamics

E. Westerhof[1], H.J. de Blank[1], R. Chandra[1], J.P. Frankemölle[1,2]

[1] *DIFFER – Dutch Institute for Fundamental Energy Research, Partner in the Trilateral Euregio Cluster, De Zaale 20, 5612 AJ Eindhoven, The Netherlands*

[2] *Eindhoven University of Technology, Eindhoven, 5600 MB, The Netherlands*

Introduction

In order to mitigate heat and particle fluxes to divertor targets, future fusion reactors will have to operate in the detached regime. Control of divertor detachment will then be essential for the safe operation. This requires knowledge or, even better, a real-time-capable model of the dynamic behaviour of divertor detachment to enable robust model-based control. With this goal in mind a 1-dimensional code has been developed to describe the dynamics of a single flux tube in the divertor leg from the X-point at the divertor entrance down to the target. Assuming equal electron and ion temperatures, the code solves the balance equations for plasma particles, momentum, and energy as well as a simple diffusion equation for the neutral particle density [1, 2] on a 1D field aligned grid running from $x = 0$ at the X-point to $x = L$ at the target. At the X-point the upstream density, $n_{\rm X}$, and the parallel heat flux $q_{\parallel,{\rm X}}$ are given whereas the momentum and neutral density are left free. At the target the Bohm condition and the sheath heat transmission are specified, i.e. the heat flux at the target is given by $q_\parallel(x = L) = \gamma n T c_{\rm s}$ where $\gamma = 6$ is the sheath heat transmission factor and the sound speed $c_{\rm s} = \sqrt{2T/m}$. The neutral particle flux coming from the target is given by a recycling coefficient times the plasma particle flux reaching the target. Sources and sinks include the effects of charge exchange, ionization, recombination, excitation, and of Carbon impurity radiation. The relevant rates are obtained from the AMJUEL data base as available on the website of the EIRENE neutral particle Monte Carlo code [3]. The Carbon impurity radiation losses are included using fits from Post et al. [4].

Steady state solutions and stability

In a first series of simulations the code is used to study steady-state conditions for MAST-Upgrade-like conditions similar to those in [2], except for the neglect of flux expansion in the present work. The length of the divertor leg is chosen as $L = 20$ m, and the parallel heat flux entering the divertor leg is set at $q_{\parallel,{\rm X}} = 50$ MW/m^2. The main plasma ion is set to deuterium with a Carbon impurity fraction of 1%. A non-equidistant grid is used with $N = 1000$ points in total and a resolution near the target of $\Delta x = 0.04$ cm. A scan of the upstream density is performed for $n_{\rm X} = 1.5$ to 5.7×10^{19} m^{-3}. The results of these simulations are presented in Figure 1a and b, representing the target density and the X-point and target temperature, respectively. At low

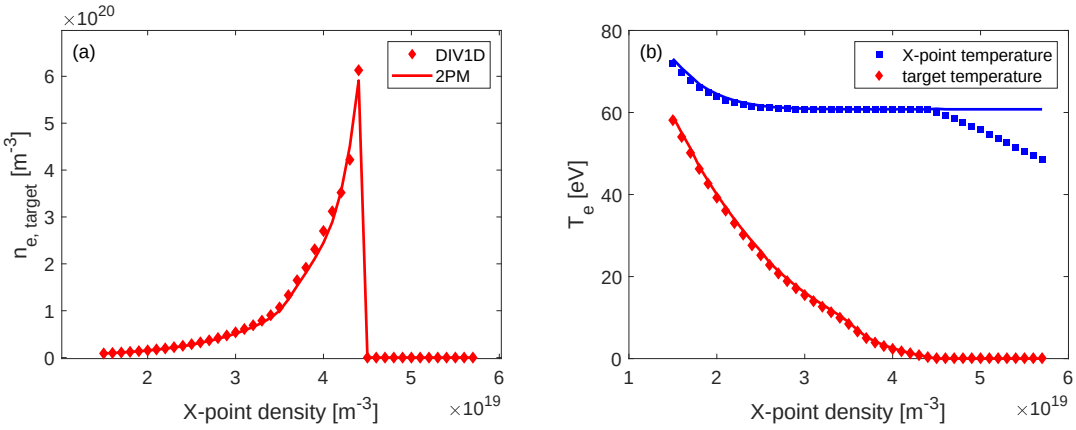

Figure 1: Results of an X-point density scan with a 1% Carbon impurity fraction. (a) Target density (diamonds) as a function of X-point density. (b) X-point (squares) and target (diamonds) temperatures. Corresponding results of the two-point model are shown as full lines.

upstream density the divertor is seen to be in the attached regime characterized by a strongly increasing target particle flux with increasing upstream density. Full detachment is achieved at densities of $n_X \geq 4.5 \times 10^{19}$ m^{-3}, where the target density and temperature have dropped to zero. This is preceded by a partially detached regime characterized by a rollover of the target particle flux at densities above $n_X = 3.6 \times 10^{19}$ m^{-3}.

As a validation of the code results a comparison is made to the predictions of the extended two-point model [5]. In the present simulations, the convected heat flux fraction f_{conv} is negligibly small by virtue of the vanishing flow at the X-point. In addition, the power and momentum loss fractions f_{pwr} and f_{mom} are obtained from the simulations. The resulting predictions of the extended two point model are indicated in Figure 1a and b by the full lines. The results of the simulations show an excellent agreement with the extended two point model, with the exception of the X-point temperatures for the fully detached cases. This is easily explained by the smaller effective divertor connection length between the X-point and the recombination front, which is now well detached from the target surface.

In cases where full detachment is achieved the recombination front is always found to be stable. This can be understood in terms of the stability criterion of radiation fronts as given by Hutchinson [7], which states that the front is stable when $\mathrm{d}(q_i - q_{\text{front}})/\mathrm{d}x_f \leq 0$, where x_f is the front position and q_i is the parallel heat flux entering the front and q_{front} represents the total energy loss in the radiation front. The latter can be written is simply proportional to the pressure p at the front location and the square root of the impurity fraction xi_Z [6, 7]: $q_{\text{front}} \propto p\sqrt{\xi_Z \int_0^\infty \sqrt{T} L_Z(T)\mathrm{d}T}$, where we have used that the parallel heat conductivity can be written as $\kappa_\parallel = \kappa_0 T^{5/2}$ and $L_Z(T)$ is the radiation loss function of the Carbon impurities. In our case, the heat flux entering the front is simply equated to $q_{\parallel,\text{X}}$ and thus independent of the

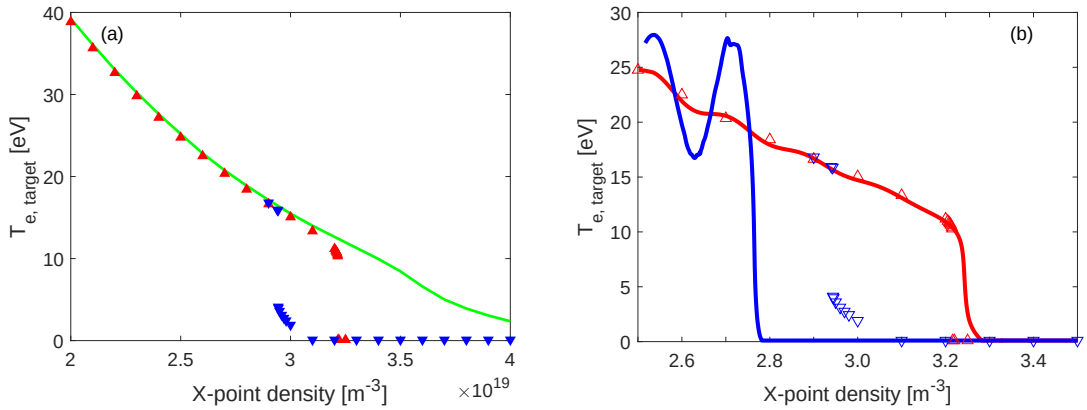

Figure 2: (a) Target temperature as function of X-point density for stationary solutions in case of a 5% Carbon impurity fraction. Red (blue) triangles correspond to solutions obtained starting from initial conditions derived from a slightly lower (higher) density. The green line represents the solutions in case of 1% Carbon. (b) Target temperature as a function of X-point density during a 10 ms density ramp (red: ramp-up and blue: ramp-down).

front position. Changing the front location x_f will, however, change the temperature and thus the pressure at the X-point and correspondingly the pressure at the front location. As a result, q_{front} will increase (decrease) as the front location x_f is increased (decreased), thus satisfying the front stability condition. Since in all fully detached cases $q_{\parallel,\text{X}} = q_{\text{front}}$ the pressure and consequently all plasma profiles are independent of the front location. When plotted relative to the front location this is indeed confirmed in the simulation results.

Bifurcations and dynamics

When the impurity fraction is increased, the non-monotonous nature of the impurity radiation function $L_Z(T)$ can give rise to the occurrence of a bifurcation in the stationary solutions for the divertor leg. According to Capes et al. [6] , the critical impurity concentration above which the stationary divertor leg solution are bifurcated scale as $\xi_\star \propto [\sqrt{T}L_Z(T)]^{-1}_{\text{max}}$. For Carbon impurity in a Deuterium plasma as above, we find a critical concentration of 2.5%. The bifurcation is indeed clearly seen in the stationary solutions as shown in Figure 2a, which shows the target temperature as a function of the X-point density in case of a Carbon concentration of 5%. In order to map out fully the high and low target temperature branches of the stationary state solutions it is was necessary to make small steps in X-point density when approaching the bifurcation point. We also demonstrate the dynamic capabilities of the code by performing density ramps between 2.5 and 3.5×10^{19} m^{-3}. Figure 2b shows the target temperature as a function of the X-point density during both a 10 ms ramp-up (red) as well as ramp-down (blue). In both cases the density varies linearly in time such that for the red curve (ramp-up) time increases to the right and for the blue curve (ramp-down) time increases to the left. The

oscillation seen in the solution for the ramp-down after the bifurcation from the low- to the high-target-temperature solution, is the result of density perturbation sloshing between target and X-point, where it is reflected due to the X-point density boundary condition.

A second use case for dynamic simulations with the 1D code is the study of the effect of ELM pulses [8]. As a first step, a simple ELM model is included in the code in which the X-point heat flux entering the divertor leg is increased linearly in time above its stationary level during a given rise time and subsequently decreased linearly back to the stationary level in a given fall time. The fall time is taken to be twice the rise time of the ELM pulse. Figure 3 shows results of a simulation of an ELM pulse for a case where the stationary solution represents a deeply detached state with the detachment front located at $x = 14.97$ m ($n_X = 5.0 \times 10^{19}$ m^{-3}, 1% C). At 1 ms in the simulation an ELM is triggered with a rise time of 250 μs and a total fluence of 140 kJ. The figure show the evolution of the parallel heat flux at different position along the divertor leg. The ELM heat flux almost instantaneously reaches the detachment front pushing it back all the way to the target resulting in re-attachment. Detachment is restored relatively quickly and the total fluence seen by the target is well below the140 kJ of the ELM itself. The recovery of the initial stationary state takes much longer as the detachment front is moving back relatively slowly.

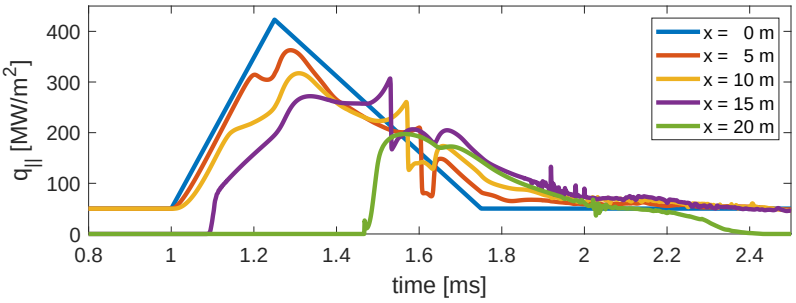

Figure 3: The parallel heat flux at different positions along the divertor leg during an ELM.

Acknowledgement This work has been carried out within the framework of the EUROfusion Consortium and has received funding from the EURATOM research and training programme 2014-2018 and 2019-2020 under grant agreement No. 633053. The views and opinions expressed herin do not necessarily reflect those of the European Commission.

References

[1] Shinji Nakazawa et al., Plasma Phys. Control. Fusion **42** (2000) 401.
[2] B.D. Dudson et al., Plasma Phys. Control. Fusion **61** (2019) 065008.
[3] `http://www.eirene.de/html/amjuel.html`.
[4] D.E. Post et al., Atomic data and nuclear data tables **20** (1977) 397.
[5] P.C. Stangeby, 2000, *The Plasma Boundary of Magnetic Fusion Devices*, IoP Publishing, UK.
[6] H. Capes, Ph. Ghendrih, and A. Samain, Phys. Fluids B **4** (1992) 1287.
[7] I.H. Hutchinson, Nucl. Fusion **34** (1994) 1337.
[8] J.P.K.W. Frankemölle, MSc Thesis TU Eindhoven (2021)
https://pure.tue.nl/ws/portalfiles/portal/168803090/0898886_Frankem_lle_J.P.K.W._MSc_thesis_MAP.pdf